CRYSTAL GROWTH & DESIGN
pubs.acs.org/crystal
Article

Effect of Substrates and Thermal Treatments on Metalorganic Chemical Vapor Deposition-Grown Sb_2Te_3 Thin Films

Martino Rimoldi, Raimondo Cecchini, Claudia Wiemer, Emanuele Longo, Stefano Cecchi, Roberto Mantovan,* and Massimo Longo*

Cite This: Cryst. Growth Des. 2021, 21, 5135–5144
Read Online

ACCESS | Metrics & More | Article Recommendations | Supporting Information

ABSTRACT: Antimony telluride (Sb_2Te_3) thin films were obtained by metalorganic chemical vapor deposition (MOCVD). The films were grown on crystalline Si(100) and Al_2O_3(0001) and amorphous SiO_2 and a-Al_2O_3 substrates. Their structural properties were compared with those of the Sb_2Te_3/Si(111) heterostructure. In addition to the effect of the substrate, the influence of pre- and post-growth thermal annealing is also presented. The quality of the films is discussed by comparing their morphological properties, such as roughness and granularity, and ascertaining their crystallinity and their in-plane and out-of-plane orientation.

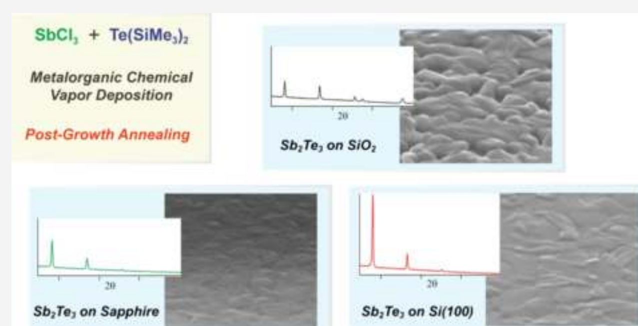

■ INTRODUCTION

Chalcogenide materials are currently foreseen to find applications in the development of emerging technologies. In particular, chalcogenide structures, such as Sb_2Te_3, Bi_2Te_3, or Bi_2Se_3, have recently been emphasized as topological insulators,[1−6] and are exploited in phase-change memories,[7,8] thermoelectric devices,[9,10] and spintronics.[11]

Either as thin films or in the form of more engineered structures such as nanowires[12−14] and multilayer stacks,[15,16] the deposition of tellurides and selenides has been achieved using a variety of physical and chemical methods, including, for instance, microwave-assisted sputtering,[16,17] solvothermal synthesis,[18] molecular beam epitaxy,[19−22] atomic layer deposition,[15,23−28] chemical vapor deposition (CVD),[29,30] and metalorganic CVD (MOCVD).[2,4,31−36] Among these methods, MOCVD, a large-scale and industrially ready technique, is capable of fabricating high-quality materials.

Trialkylstibines (such as $SbMe_3$ and Sb^iPr_3) and dialkyltellanes ($TeEt_2$ and Te^iPr_2) are well-exploited MOCVD precursors, commonly requiring high deposition temperatures (up to 450 °C) and a dihydrogen atmosphere.[32,34]

Taking advantage of the reactivity of $SbCl_3$ (antimony chloride) and $Te(SiMe_3)_2$ (bis(trimethylsilyl)telluride), originally reported in the atomic layer deposition of tellurides,[15,23,24] their use as precursors in a room-temperature (RT) MOCVD to grow Sb_2Te_3 thin films has been proven.[4,37,38]

So far, the epitaxial growth of Sb_2Te_3 has been demonstrated by molecular beam epitaxy on Si(111) and BaF_2,[21,22,39] pulsed laser deposition on Si(111),[40] thermal evaporation on Al_2O_3(0001),[41] and MOCVD on Si(111) as well as on ZnTe buffer layers.[34,38,42]

An efficient growth of topological insulators on crystalline silicon substrates, such as Si(111) or Si(100), would be attractive for their compatibility with the complementary metal-oxide semiconductor (CMOS) technology.[43,44] However, in view of the integration of TI-based components into electronic devices, it is pivotal to study their growth behavior on oxides (SiO_2 and Al_2O_3),[45,46] as they are relevant, for instance, to develop thermoelectric materials, to investigate the topological states at the interface with the substrate,[47] or to allow back-gating.[48]

The crystallinity and the morphological quality are relevant evaluation criteria. From an application perspective, achieving highly oriented Sb_2Te_3 films is mandatory: a controlled out-of-plane orientation, that is, a *c*-oriented thin film or even the ability to attain an epitaxial growth is an essential prerequisite to best exploit their physical properties as topological insulators. In fact, as recently reported, it allowed spin-to-charge conversion, as probed by spin-pumping ferromagnetic resonance.[44] In addition, control over the surface roughness and granularity (morphological quality) is essential when producing, for instance, technologically relevant multilayered materials to optimally interface topological insulators with

Received: May 1, 2021
Revised: July 19, 2021
Published: July 29, 2021

Downloaded via UNIV DEGLI STUDI DI TOR VERGATA on January 18, 2024 at 15:02:01 (UTC).
See https://pubs.acs.org/sharingguidelines for options on how to legitimately share published articles.

ACS Publications © 2021 American Chemical Society

Table 1. Sb_2Te_3 Root Mean Square Roughness (R_q, nm), Measured by AFM and XRR, and Thickness (nm), Determined by XRR

	Sb_2Te_3 - as-deposited			Sb_2Te_3 - substrate annealing (prior to growth)			Sb_2Te_3 - post-growth annealing		
	$R_{q\ (AFM)}$	$R_{q\ (XRR)}$	thickness $_{(XRR)}$	$R_{q\ (AFM)}$	$R_{q\ (XRR)}$	thickness $_{(XRR)}$	$R_{q\ (AFM)}$	$R_{q\ (XRR)}$	thickness $_{(XRR)}$
Si(111)[a]	3.88	3.1	33.7	1.81	2.0	32.5	1.32	1.5	32.0
Si(100)	4.80	4.6	33.7	2.78	3.4	31.0	2.26	2.6	31.7
SiO_2	2.41	3.1[b]	35.0[c]	4.90	6.6	30.9	5.51	4.5	32.4
a-Al_2O_3	3.40	3.3[d]	32.2	3.61	4.1[e]	29.0	3.07	3.4[f]	27.5
Al_2O_3(0001)	1.94	2.6	28.8	3.25	3.9[g]	28.2[h]	2.18	3.3[i]	25.2[j]

[a]Si(111) is reported for comparison purpose.[38] [b]Sb_2O_3 interlayer roughness: 0.4 nm. [c]Sb_2O_3 interlayer thickness: 2.0 nm. [d]a-Al_2O_3 roughness: 0.5 nm. [e]a-Al_2O_3 roughness: 0.4 nm. [f]a-Al_2O_3 roughness: 0.5 nm. [g]Sb_2O_3 interlayer roughness: 0.1 nm. [h]Sb_2O_3 interlayer thickness: 0.5 nm. [i]Sb_2O_3 interlayer roughness: 0.1 nm. [j]Sb_2O_3 interlayer thickness: 0.3 nm.

metallic or ferromagnetic layers.[5] Lastly, resistivity is a preliminary, nevertheless essential evaluation parameter for thermoelectric materials.

Here, we report our recent investigation on the deposition of Sb_2Te_3 thin films by RT MOCVD. Our systematic study revealed a uniform growth on a variety of substrates, a crucial feature for further improvements. Building on the good quality of the RT films, we focused on the morphological and structural changes induced by pre- and post-growth thermal annealing and, particularly, on the effect of the substrate. Ultimately, we identified highly oriented crystalline Sb_2Te_3 films, their morphological improvements, and conducted RT resistivity measurements to functionally characterize a structurally broad set of thin films.

EXPERIMENTAL SECTION

Materials. Si(111), Si(100), and SiO_2 (nominal 50 nm thermal oxide on Si(100)) wafers were acquired from Silicon Materials Inc. and Al_2O_3(0001) from CrysTec GmbH. Amorphous Al_2O_3 (a-Al_2O_3) thin films (thickness of ca. 10 nm) were prepared by atomic layer deposition on SiO_2 (nominal 50 nm thermal oxide on Si(100)) in a Savannah 200 reactor using TMA (trimethylaluminum) and H_2O as aluminum and oxygen sources, respectively; the deposition was carried out at 150 °C, according to the following parameters: TMA pulse time: 0.05 s, TMA purge time: 45 s, H_2O pulse time: 0.2 s, H_2O purge time: 45 s, and number of cycles: 100. Substrates were cut to approximately 1 to 2 cm^2 pieces.

Sb_2Te_3 Thin Films by MOCVD. Prior to deposition, the Si(111) and Si(100) substrates were treated with hydrofluoric acid (5% in deionized water) for 3 min, thoroughly rinsed with deionized H_2O, and N_2-dried; the a-Al_2O_3 substrates were freshly prepared prior to MOCVD growth. After preparation, the substrates were quickly transferred into a glovebox-protected MOCVD chamber. Sb_2Te_3 thin films were grown with an Aixtron AIX 200/4 MOCVD tool, equipped with an IR-heated 4″ rotating graphite susceptor. Electronic-grade MOCVD precursors $SbCl_3$ and $Te(SiMe_3)_2$ were provided by Air Liquide Electronics. Precursors were contained into bubblers thermalized at 20.0 ± 0.1 °C and delivered to the MOCVD chamber through the vapor-saturated ultrapure N_2 carrier gas. Typically, the Sb_2Te_3 growths were performed after conditioning the deposition chamber with Sb_2Te_3 deposition runs. If needed, prior to the conditioning runs, a prolonged high-temperature bake-out (700 °C, 3 h) was performed to free the chamber from residues of other deposition processes, thus preventing memory effects. The MOCVD setup in use is designed to mix the precursors nearby the graphite sample holder to inhibit "premature reactions." In addition, we did not have signs of parasitic depositions. Depositions were carried out for 90 min at 25 °C and 15 mbar pressure, with a total flow of 5.575 L/min and by setting the vapor pressure of $SbCl_3$ and $Te(SiMe_3)_2$ at 2.28 and 3.32 10^{-4} mbar, respectively. Substrate annealing (prior to deposition) was performed in situ for 60 min at 500 °C and 20 mbar, with a total N_2 flow of 11.000 L/min. Post-growth film annealing was performed in situ according to the following routine: (1) heating ramp: 5.575 L/min N_2 flow, 900 mbar, from RT to 300 °C in 10 min; (2) annealing: 5.575 L/min N_2 flow, 900 mbar, 300 °C, 15 min; (3) cooling ramp: 1.500 L/min N_2 flow, 990 mbar, from 300 to 200 °C in 20 min, from 200 to 100 °C in 35 min, from 100 to 50 °C in 20 min.

Material Characterization. Scanning electron microscopy (SEM) images were acquired with a ZEISS Supra40 field-emission scanning electron microscope, operating at an acceleration voltage of 15 kV; cross-section images were collected at a tilting angle of 25°. Atomic force microscopy (AFM) measurements were acquired on a Bruker Dimension Edge instrument in the noncontact mode using AFM silicon probes (TESPA, Bruker). The surface roughness was expressed as root mean square roughness (RMS Roughness, R_q). Total reflection X-ray fluorescence (TXRF) measurements were performed using an X-ray total reflection spectrometer equipped with a Mo Kα radiation source. Elemental compositions were obtained from the ratio of the antimony and tellurium Lα lines (Sb Lα = 3.604 keV; Te Lα = 3.768 keV). X-ray reflectivity (XRR) and X-ray diffraction (XRD) patterns were acquired with a HRXRD IS2000 diffractometer equipped with a Cu Kα radiation source, a four-circle goniometer, and a curved 120° position-sensitive detector. Electrical resistivity (ρ) was measured with a custom-made four-point van der Pauw setup in vacuum (base pressure = 10^{-5} mbar), on 1 × 1 cm^2 samples. Intrinsic substrates (with ρ > 10,000 Ω·cm) were used for the electrical measurements of the Sb_2Te_3 films grown on crystalline silicon.

RESULTS AND DISCUSSION

To establish the effect of the substrate on directing the MOCVD of the Sb_2Te_3 thin films, we explored the use of crystalline and amorphous substrates. Among these, sapphire has recently been found suitable for good-quality and highly crystalline telluride thin film preparation by thermal evaporation,[41] whereas SiO_2 has been used to successfully produce out-of-plane oriented Sb_2Te_3 films by sputtering.[49]

Taking advantage of the optimization achieved in the growth of Sb_2Te_3 by MOCVD on Si(111),[38] in addition to the substrate assessment, we examined the effect of thermal treatments on the bare substrates (substrate annealing prior to deposition) and on the deposited thin films (post-growth annealing).

The chemical reactivity of $SbCl_3$ and $Te(SiMe_3)_2$ allowed exploiting the RT antimony telluride deposition, rather than a high-temperature pyrolysis-driven process; it is worth mentioning that the same set of precursors could be used in a high-temperature MOCVD: upon varying the temperature of the growth, within the 100−250 °C range, changes were induced on the granularity and overall morphology of the films (Figure S1, Supporting Information).[37] Nevertheless, the best quality was achieved via the RT MOCVD growth, followed by the substrate annealing and the post-growth annealing steps.

https://doi.org/10.1021/acs.cgd.1c00508
Cryst. Growth Des. 2021, 21, 5135−5144

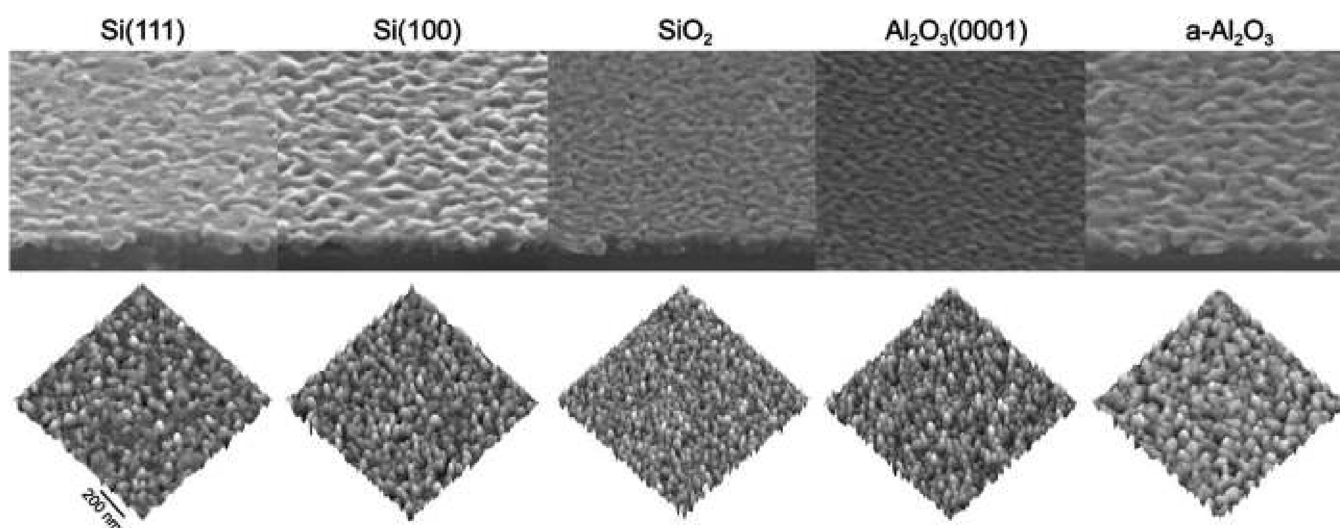

Figure 1. (top) Tilted cross-section SEM images and (bottom) AFM views of Sb_2Te_3 - *as-deposited* on (from left to right) Si(111), Si(100), SiO_2, Al_2O_3(0001), and a-Al_2O_3. Si(111) is reported for comparison purpose.[38] As-deposited films appeared to have a pronounced granularity. However, those grown on SiO_2 and Al_2O_3(0001) were significantly smoother and gave AFM R_q values of 2.41 and 1.94 nm, respectively.

Under the adopted RT experimental conditions, that consisted of $SbCl_3$ and $Te(SiMe_3)_2$ partial pressures set to 2.23×10^{-4} and 3.25×10^{-4} mbar, respectively, a total flow of 5.575 L min^{-1}, and a chamber pressure of 15 mbar, the process yielded, at a deposition time of 90 min, films in the thickness range from 29 to 35 nm, depending on the substrate of choice. As a general trend, a slight thickness reduction was observed on the films subjected to the annealing processes (see Table 1).

Commonly, deposition parameters, such as the deposition temperature and the precursor partial pressure, are tuned to favor the coalescence of the film and control its growth and crystallinity, but this can alter the stoichiometry of the films.[33,34] In contrast, through our study, the stoichiometry of the films, probed by total reflection X-ray fluorescence spectroscopy, was constantly found to be $Sb_{2.0}Te_{3.0}$, regardless of the substrate or thermal annealing. In fact, we maintained the growth conditions constant and regulated the morphological quality of the film through the pre-growth and post-growth conditions.

Sb_2Te_3 - *As-Deposited*. The Sb_2Te_3 - *as-deposited* films (annealing not applied to these materials) were obtained with a pronounced granularity; however, when grown on SiO_2 and Al_2O_3(0001), they appeared appreciably smoother (Figure 1). Their surface roughness (AFM R_q values of 2.41 and 1.94 nm for Sb_2Te_3/SiO_2 and Sb_2Te_3/Al_2O_3(0001), respectively) was significantly lower compared to that of the films deposited on other substrates (Table 1; Figure S2, Supporting Information), including Sb_2Te_3/Si(111).[38] Instead, their thickness, probed by XRR, was 35.0 and 28.8 nm for Sb_2Te_3/SiO_2 and Sb_2Te_3/Al_2O_3(0001), respectively, values comparable with those of the films grown on the other substrates (Table 1). The average Sb_2Te_3 growth rate has been determined on Si(111) to be approximately 0.4 nm/min,[38] a value appreciably low if compared with the MOCVD growth rate of other highly crystalline Sb_2Te_3 thin films that were reported to fall within the 8−50 nm/min range.[2,34] Such a discrepancy can be straightforwardly attributed to the adopted experimental conditions, including different precursors, high deposition temperature (up to 450 °C), and use of a dihydrogen partial pressure.

XRR analyses confirmed the AFM roughness trend and indicated sapphire to favor the higher-quality Sb_2Te_3 - *as-deposited* thin film—as inferred from the electronic density and surface roughness values. Noteworthy, an optimal XRR model of Sb_2Te_3/SiO_2 required a 2 nm Sb_2O_3 interlayer,[4] a component not needed with the other films (Table 1; Figure S3, Supporting Information).

Irrespective of the substrate used, the Sb_2Te_3 - *as-deposited* thin films exhibited a relatively similar structural quality, as ascertained by the shape and position of the peaks in the grazing incidence X-ray diffractograms (Figure 2).

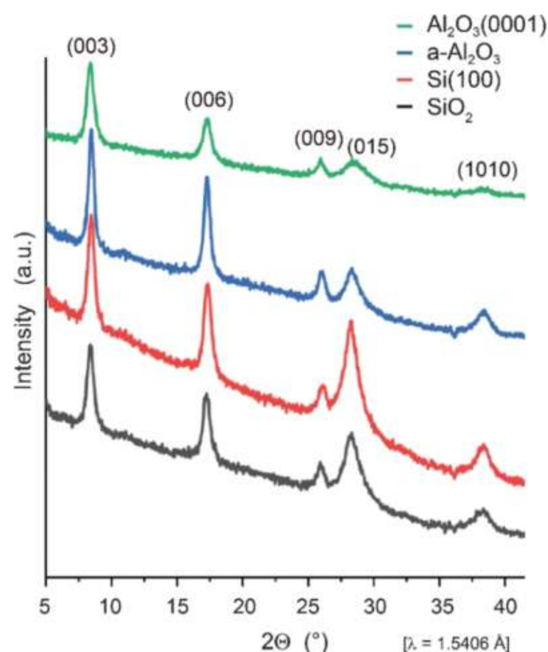

Figure 2. Grazing incidence XRD pattern of Sb_2Te_3 - *as-deposited* on (black) SiO_2, (red) Si(100), (blue) a-Al_2O_3, and (green) Al_2O_3(0001). The intensity, broadening, and position of the peaks are informative of Sb_2Te_3 films relatively similar in structure, regardless of the selected substrate.

https://doi.org/10.1021/acs.cgd.1c00508
Cryst. Growth Des. 2021, 21, 5135−5144

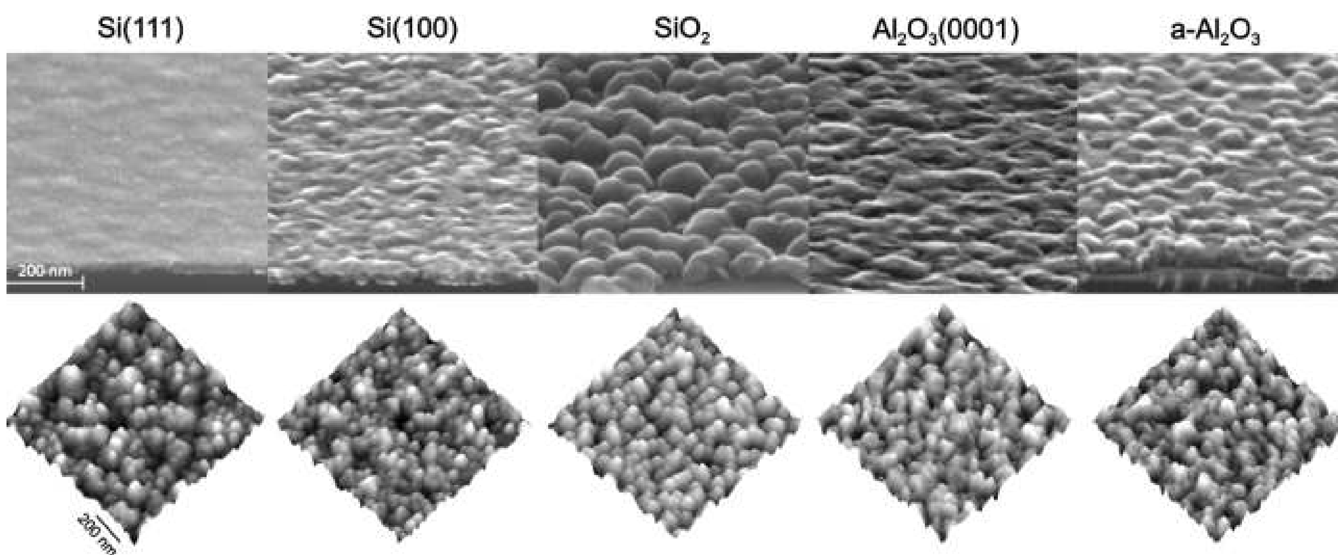

Figure 3. (top) Tilted cross-section SEM images and (bottom) AFM views of Sb_2Te_3 - *substrate annealing* on (from left to right) Si(111), Si(100), SiO_2, Al_2O_3(0001), and a-Al_2O_3. Si(111) is reported for comparison purpose.[38] The SEM images revealed the effect of substrate annealing on the morphology of the Sb_2Te_3 thin films. The granularity, and consequently the roughness, significantly improved on Si(100) and Si(111), whereas it worsened on SiO_2.

However, the sharper and more intense (00l) peaks in Sb_2Te_3/a-Al_2O_3 and Sb_2Te_3/Al_2O_3(0001) indicated an overall higher crystallinity, as well as crystallites bigger in size and likely out-of-plane oriented along the [00l] direction. On the other hand, the more intense and broader (015) reflection in the diffraction patterns of Sb_2Te_3/Si(100) and Sb_2Te_3/SiO_2 revealed their greater random and polycrystalline nature and possibly amorphous fractions. The XRD analysis in the Bragg–Brentano geometry showed mostly the (00l) reflections only, further supporting that the Sb_2Te_3 films are mostly (00l) out-of-plane-oriented. From the rocking curve around the (006) reflection of Sb_2Te_3/a-Al_2O_3, a mosaicity of approximately 4° was calculated. This value is lower than that measured on Sb_2Te_3/Si(111) (9°),[38] revealing a higher order of the (00l) crystallites. Nevertheless, the (00l) reflections are very weak, and their broadening along the ω direction indicated a still high mosaicity (Figure S4, Supporting Information). Further investigations found no presence of any in-plane order.

Sb_2Te_3 - *Substrate Annealing*. Substrate annealing (i.e., pre-growth thermal annealing of substrates) was performed in situ at 500 °C and at a reduced pressure (20 mbar), whereas the subsequent MOCVD process was conducted at RT. The annealing has been previously investigated in related chalcogenide materials:[50,51] in the MOCVD of Ge-Sb-Te thin films, substrate annealing has been essential to control the morphology and achieve layer coalescence. This pre-growth process, however, has been conducted in a pure dihydrogen atmosphere, known to support the Ge-Sb-Te growth,[50] and, more importantly, along with the injection of the tellurium precursor to favor the van der Waals epitaxy.[51] Differently, the substrate annealing adopted here is simply based on a thermal treatment under reduced nitrogen pressure, therefore, in a nonreactive atmosphere.

The substrate annealing had a marked effect on the morphology of the films grown on all the tested substrates (Figure 3). The thicknesses of Sb_2Te_3/Si(100) and Sb_2Te_3/SiO_2, respectively, 31.0 and 30.9 nm, were slightly reduced as compared to the as-deposited analogues; the granularity appreciably improved on the crystalline substrate Si(100), as also previously observed on Si(111),[38] resulting in a more continuous and uniform film with a lowered surface roughness (RMS R_q of 2.8 nm).

In contrast, substrate annealing did not prove to be just as much effective on the two aluminum oxide substrates. Even though grain cohesion was enhanced to such an extent that the films appeared continuous, clearly visible from the SEM observations (detailed in Figure 3), their roughness instead worsened to 3.6 and 3.3 nm for Sb_2Te_3/a-Al_2O_3 and Sb_2Te_3/Al_2O_3(0001), respectively (Table 1). The thicknesses of the films were 29.0 and 28.2 nm on a-Al_2O_3 and Al_2O_3(0001), respectively.

On the other hand, the substrate annealing exhibited a drastically reverse effect, once applied to the SiO_2 substrate: the deposited Sb_2Te_3 material formed islands approximately 100 nm in size; hence, it no longer qualifies as a film. XRR analyses outlined that, different from the Sb_2Te_3/SiO_2 - *as-deposited* film, the Sb_2O_3 interlayer was not present; in fact, the substrate annealing is expected to readily remove strongly adsorbed water and significantly reduce silanols—features accountable for the formation of the detected low-density layer (Table 1; Figure S3, Supporting Information). Upon modeling the Sb_2Te_3/Al_2O_3(0001) XRR data, instead, a very thin (0.5 nm) interlayer, whose electronic density is compatible with the Sb_2O_3 chemical composition, has to be accounted for.

Roughness-wise, XRR measurements outlined that, except the Sb_2Te_3/Si case, the substrate annealing step unfavorably affected the growth of the films, particularly on SiO_2.

Pre-growth annealing performed at moderate temperatures is commonly expected to free the substrate from adsorbates: because of the highly protolyzable organometallic precursor used, annealing is thought to be mainly relevant in removing physisorbed and chemisorbed water. Consequently, we speculate that the change in roughness and granularity induced by the pre-growth annealing results from different incipient reactions occurring at the annealed substrates, rather than at the untreated substrates. Moreover, the various tested substrates inherently exhibited dissimilar behaviors: in fact, we observed interlayers formed on some substrates and under

https://doi.org/10.1021/acs.cgd.1c00508
Cryst. Growth Des. 2021, 21, 5135−5144

certain conditions (see Table 1), suggesting that a different chemical affinity between the substrate and the precursors directs the deposition process, therefore influencing the final morphology of the films.

The crystallinity appeared enhanced in all the films grown on annealed substrates, except SiO_2. In the latter, the total absence of the (00l) reflections indicated randomly oriented crystallites (Figure 4), and the Bragg−Brentano analyses further confirmed the absence of an out-of-plane ordering due to randomly oriented crystallites (Figure S5, Supporting Information)—a description that matches well the clustering observed by SEM (Figure 3).

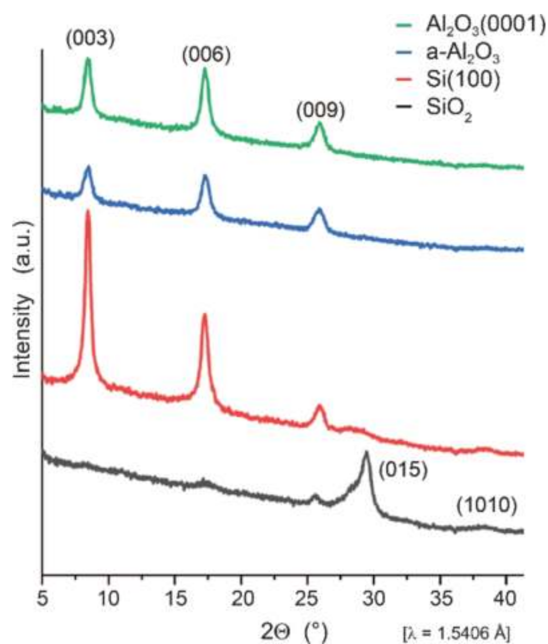

Figure 4. Grazing incidence XRD pattern of Sb_2Te_3 - *substrate annealing* on (black) SiO_2, (red) Si(100), (blue) a-Al_2O_3, and (green) Al_2O_3(0001). Substrate annealing enhanced the crystallinity of the Sb_2Te_3 thin films on each substrate, except SiO_2. The Sb_2Te_3/Si(100) film is the most out-of-plane-oriented, even though weak reflections that do not belong to the (00l) family still suggest a polycrystalline nature and an amorphous fraction.

The substrate annealing favored a general out-of-plane orientation of the Sb_2Te_3 film along the [00l] direction both on a-Al_2O_3 and Al_2O_3(0001), as confirmed by the almost total absence of reflections pertaining to different crystalline planes (Figure 4; Figure S5, Supporting Information). However, the intensity ratio of the (003) and (006) reflections did not correspond to the one reported in database,[52] suggesting a different texturing and/or a nonoptimal crystallization of the film.

The Sb_2Te_3/Si(100) structure appeared to be the most out-of-plane-ordered: the high and sharp 00l peaks indicated larger crystallites (Figure 4), whereas the presence of a faint but broadened 015 peak and further reflections not belonging to the (00l) family of planes revealed a polycrystalline nature and amorphous fractions, features instead not observed in Sb_2Te_3/Si(111). An XRD scan of the azimuthal angle (Φ) performed on the (015) reflection of the (00l) out-of-plane oriented crystallites highlighted equally spaced peaks at 2Θ = 28°, indicative of a certain degree of the in-plane order (Figure 5; Figure S6, Supporting Information).

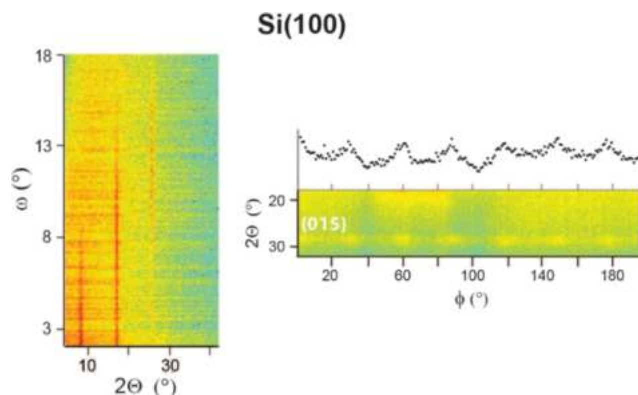

Figure 5. XRD maps (left) in the Bragg−Brentano geometry and the (right) ϕ angle scans of Sb_2Te_3 - *substrate annealing* on Si(100). The scan of the azimuthal angle indicates a degree of the in-plane order.

The threefold symmetry of the rhombohedral Sb_2Te_3 cell would ideally provide three 60°-spaced peaks, as found in Sb_2Te_3/Si(111). The occurrence of six 30°-spaced peaks is therefore rationalized as two families of crystallites, whose (015) reflections are 30° offset in-plane.

Sb_2Te_3 - Post-Growth Annealing. The quality of the Sb_2Te_3 thin films grown by RT MOCVD was effectively improved by post-growth annealing.[38] We applied the same protocol on all the Sb_2Te_3 - *substrate annealing* films and found that the surface roughness generally diminished, as probed by AFM and XRR analyses, to values as low as 2.2 and 2.3 nm on the crystalline Al_2O_3(0001) and Si(100) substrates, respectively (see Table 1; Figure S3, Supporting Information). The thickness of the films slightly increased on Si(100) and SiO_2 (Table 1), whereas it showed a more marked decrease on the two aluminum oxide substrates (27.5 and 25.2 nm for Sb_2Te_3/a-Al_2O_3 and Sb_2Te_3/Al_2O_3(0001), respectively).

Interestingly, the XRR model of the Sb_2Te_3/Al_2O_3(0001) heterostructure still evidenced an interlayer, thinner (0.3 nm) and denser than the one observed in the *substrate annealing* analogue, and suggestive of an intermixing between the Sb_2Te_3 film and the sapphire surface.

The thermal processing favored the crystallization of the films: the SEM and AFM images (Figure 6) highlighted the high crystallinity and the extent of the film orientation.

In Sb_2Te_3/SiO_2 - *post-growth annealing*, it is evident that the highly granular nature was retained, reflecting the granularity of the parent samples, but the isolated grains underwent marked crystallization (Figures 3 and 6).

The intensity and sharpness of the 00l peaks in the grazing incidence XRD patterns (Figure 7) demonstrated an improved crystallinity, as result of a higher fraction of crystallites oriented along the [00l] direction, except for the Sb_2Te_3/SiO_2 thin film that was instead characterized by the (015) and (1010) reflections, thus revealing a polycrystalline component.

The combined XRD measurements in the Bragg−Brentano geometry and the ϕ angle scans indicated that the films grown on the amorphous a-Al_2O_3 and SiO_2 were poorly oriented. In fact, the peaks highly broadened along ω (Figure 8) and the continuous and faint line detected at 2Θ = 28° in the ϕ angle scans (Figure S7, Supporting Information) indicated only partially (00l) out-of-plane-oriented crystallites, with an almost random in-plane orientation. Therefore, the thermal treatment just induced a partial reorientation of the Sb_2Te_3 grains to form highly texturized films along the out-of-plane [00l] direction.

https://doi.org/10.1021/acs.cgd.1c00508
Cryst. Growth Des. 2021, 21, 5135−5144

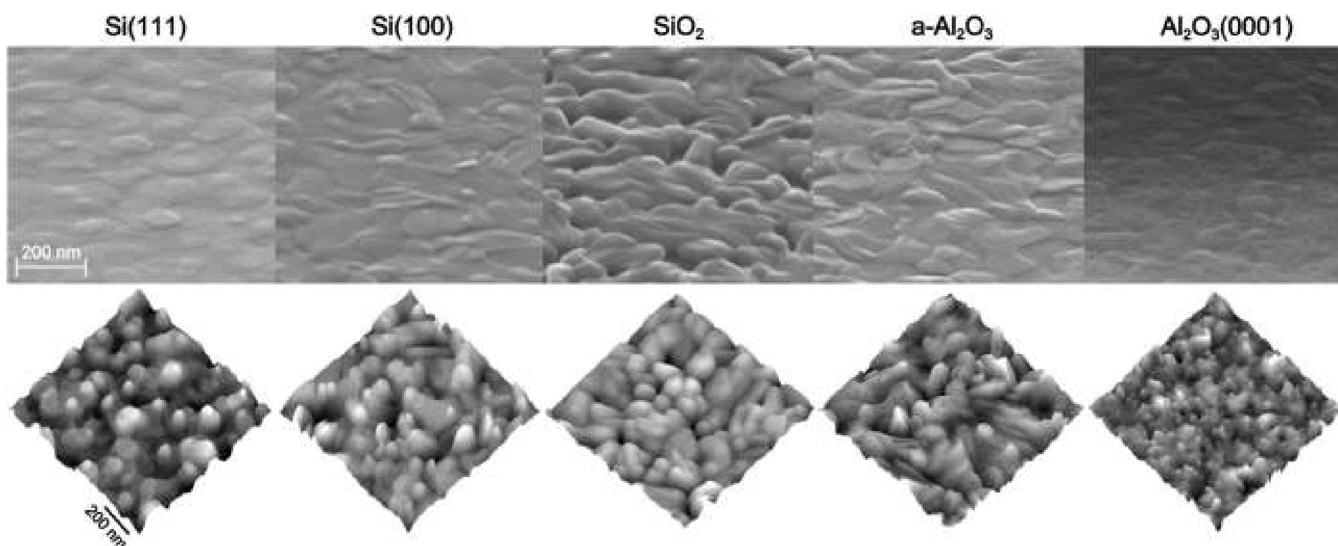

Figure 6. (top) Tilted cross-section SEM images and (bottom) AFM views of Sb_2Te_3 - *post-growth annealing* on (from left to right) Si(111), Si(100), SiO_2, a-Al_2O_3, and Al_2O_3(0001). Si(111) is shown for comparison purpose.[38] Thermal processing (post-growth annealing) induced the crystallization of the Sb_2Te_3 thin films. SEM and AFM images show the highly crystalline nature and the orientation of the films.

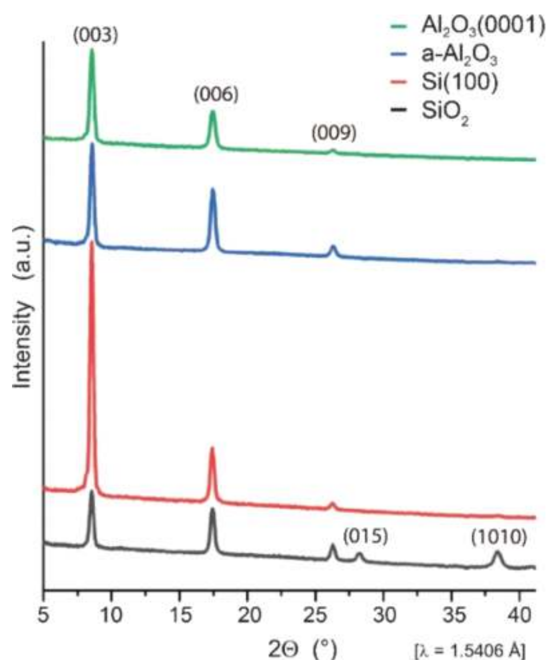

Figure 7. Grazing incidence XRD pattern of Sb_2Te_3 - *post-growth annealing* on (black) SiO_2, (red) Si(100), (blue) a-Al_2O_3, and (green) Al_2O_3(0001). The intense and sharp 00l peaks indicate highly crystalline and highly 00l-oriented crystallites; however, the Sb_2Te_3/SiO_2 structure is still characterized by the (015) and (1010) reflections that indicate a polycrystalline nature.

On the other hand, sapphire and Si(100) favored a more ordered structure. In Sb_2Te_3/Al_2O_3(0001), the rocking curve of the (006) reflection appeared very narrow, with a mosaicity of 0.15°, and most likely superimposed on a much broader, but extremely weak peak that could indicate an additional family of less out-of-plane-oriented crystallites. The Bragg−Brentano XRD data of Sb_2Te_3/Si(100) revealed instead a mosaicity of approximately 1.5° (Figure 9a).

Sb_2Te_3/Al_2O_3(0001) was characterized by three 60°-spaced peaks in the ϕ angle scan, typical of the symmetry of the rhombohedral Sb_2Te_3 crystalline structure (Figure 9b); the lower intensity of the peak positioned at ϕ = 90° can be explained with the coexistence of two not equally populated families of Sb_2Te_3 crystals offset in-plane of 60°, as previously proposed.[53]

The ϕ angle scan, where Φ = 0° corresponds to the direction parallel to Al_2O_3[110] (Figure 9b), allowed to determine the epitaxial relationships between the Sb_2Te_3 - *post-growth annealing* film and the Al_2O_3(0001) substrate: these relations can be written as Sb_2Te_3[00l]||Al_2O_3[00l] and Sb_2Te_3[015]||Al_2O_3[110]. The low mosaicity value, along with an in-plane ordering, supported the formation of an epitaxial Sb_2Te_3 film in Sb_2Te_3/Al_2O_3(0001). Nevertheless, the epitaxy is corroborated by the relatively limited 10.7% mismatch between the film and substrate in-plane lattice parameters (a_{Sb2Te3} = 4.25 nm and $a_{Al2O3(0001)}$ = 4.76 nm).

In Sb_2Te_3/Si(100), instead, the mutual crystallographic orientations between the film and the substrate could not be straightforwardly identified. Consistent with its parent *substrate annealing* sample, the XRD ϕ angle scan showed six 30°-spaced peaks (Figure 9b), suggesting two families of crystalline Sb_2Te_3 grains. One of these, linked to a ϕ angle spacing of 60°, was identified by the orientations Sb_2Te_3[00l]||Si(100)[100] and Sb_2Te_3[015]||Si(100)[110], whereas the other one, while sharing the same out-of-plane orientation, was additionally rotated in-plane of 30°, with respect to the Si(100)[110] direction. As a result of commensurability considerations and given the two Sb_2Te_3 in-plane crystalline orientations, an epitaxy definition was not fully applicable. Moreover, the scattered intensity connecting the six 30°-spaced Sb_2Te_3/Si(100) reflections indicated a non-negligible contribution from random in-plane orientations of the Sb_2Te_3 crystallites (Figure 9b), causing in-plane structural disorders on the Si(001) surface.

For a thorough description of the substrate effects on the Sb_2Te_3 growth, we would recall that the Sb_2Te_3 - *post-growth annealing* on Si(111), characterized by a mosaicity of 0.46° and an almost perfect in-plane orientation, has been described by the epitaxial relationship Sb_2Te_3[00l]||Si[111] and Sb_2Te_3[015]||Si[011].[38]

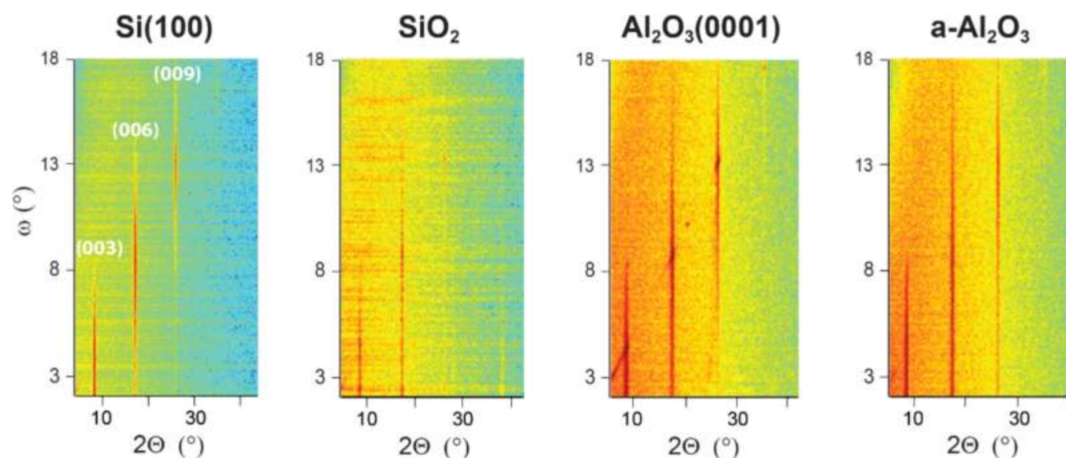

Figure 8. XRD maps in the Bragg−Brentano geometry of Sb_2Te_3 - *post-growth annealing* on Si(100), SiO_2, Al_2O_3(0001), and a-Al_2O_3. The intensity and the broadening of the 00l peaks are informative of the out-of-plane orientation of the crystallites.

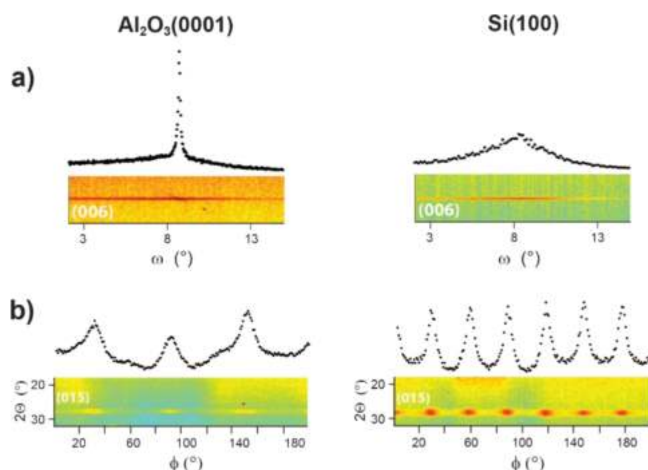

Figure 9. (a) Profiles of the 006 peak along ω extracted from the XRD measurements in the Bragg−Brentano geometry and (b) profiles of the ϕ angle scans of Sb_2Te_3 - *post-growth annealing* on (left) Al_2O_3(0001) and (right) Si(100). Among the tested substrates, sapphire and Si(100) favored the more ordered Sb_2Te_3 films. The rocking curve of the (006) reflection in Sb_2Te_3/Al_2O_3(0001) and in Sb_2Te_3/Si(100) indicated a mosaicity of 0.15 and 1.5°, respectively. The ϕ angle scans showed an in-plane order and allowed to determine the epitaxial relations in Sb_2Te_3/Al_2O_3(0001).

Therefore, the threefold symmetry of the Si(111) and Al_2O_3(0001) surfaces favors the formation of highly ordered Sb_2Te_3 crystallites, fixing their orientation in both the in-plane and out-of-plane directions.

Electrical Resistivity Measurements. The resistivity values of the Sb_2Te_3 films grown on all the different substrates, as obtained using the van der Pauw method, are reported in Figure 10 and Table 2.

The general trend over all the thin films indicated a decrease in resistivity from the *as-deposited* to the *post-growth annealing* Sb_2Te_3 films (Figure 10). Among the *as-deposited* films, lower resistivity was measured on the Sb_2Te_3 prepared on silicon oxide and aluminum oxides (4.9, 5.0, and 4.8 mΩ cm), consistently with their lower roughness (respect to Sb_2Te_3/Si films), a property that could be causally related to the homogeneity of the film and the orientation of its crystallites.

Compared with their *as-deposited* analogues, the two Sb_2Te_3/Al_2O_3 - *substrate annealing* films were characterized by a slight increase in resistivity because of their partially reduced structural order, whereas the Sb_2Te_3/Si - *substrate annealing* films, in agreement with their better crystallinity, showed lower resistivity. On the other hand, the resistivity of the Sb_2Te_3/SiO_2 film increased considerably from 4.9 to 58 mΩ cm. In fact, not only it was found to be the less crystalline among all the samples but also it was found to be highly discontinuous. A common trend, however, is observed within the *post-growth annealing* series of the films: all of them

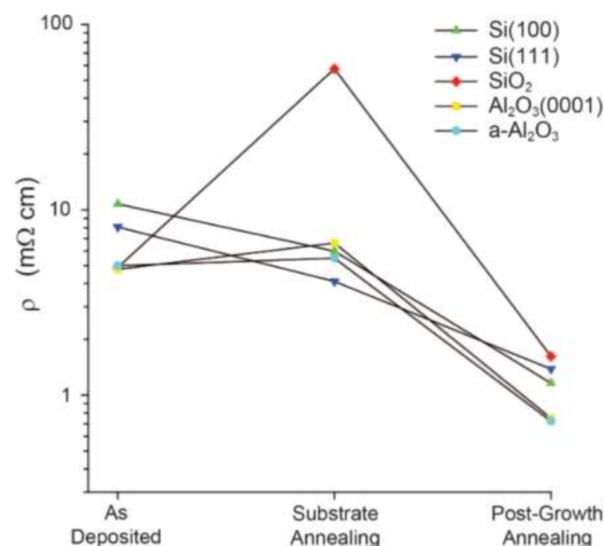

Figure 10. RT electrical resistivity of Sb_2Te_3 - *as-deposited*, *substrate annealing*, and *post-growth annealing* grown on (green) Si(100), (blue) Si(111), (red) SiO_2, (yellow) Al_2O_3(0001), and (cyan) a-Al_2O_3. As a general trend, the resistivity decreased when the *substrate annealing* and *post-growth annealing* were applied.

Table 2. Electrical Resistivity (mΩ cm) of the Sb_2Te_3 Thin Films

	as-deposited	substrate annealing	post-growth annealing
Si(111)	8.1	4.1	1.4
Si(100)	10.8	6.0	1.2
SiO_2	4.9	58	1.6
a-Al_2O_3	5.0	5.5	0.7
Al_2O_3(0001)	4.8	6.6	0.8

https://doi.org/10.1021/acs.cgd.1c00508
Cryst. Growth Des. 2021, 21, 5135−5144

demonstrated a significant drop in resistivity, a result of their enhanced crystallinity and orientation.

■ CONCLUSIONS

We developed by MOCVD a set of Sb_2Te_3 thin films exploiting the influence of substrates and thermal treatments. The tested substrates, amorphous and crystalline silicon- and aluminum-based materials, as well as the substrate annealing and post-growth processing protocols were found to be crucial in directing the nature and the properties of the films. Our results showcase a significant improvement in the preparation of highly crystalline and highly oriented chalcogenide films using a chemical method, and we can envisage that an analogous approach could be extended to other classes of chalcogenide materials.

As a trend, from the *as-deposited* to the *post-growth annealing* series of films, the surface roughness and the granularity improved significantly with each substrate, apart from SiO_2.

Generally, the post-growth thermal annealing induced the crystallization of Sb_2Te_3 on each of the tested substrates and was also highly effective in influencing the in-plane and out-of-plane orientations of the film. In particular, the most intriguing results were obtained on the crystalline substrate Al_2O_3(0001), which promoted both an in-plane and out-of-plane orientation, as observed in a similar fashion on Si(111). The extent of crystallization and ordering was first originated from the structural and morphological changes induced by Sb_2Te_3 substrate annealing. Therefore, the choice of the substrate and the substrate annealing step appeared as an essential prerequisite. Evaluating the effect of annealing and identifying the films of higher quality on each substrate allows selecting the preferred growth conditions for a specific application.

Ultimately, the electrical resistivity was found to be qualitatively consistent with the overall structural features of the set of Sb_2Te_3 films, linking their structural and functional properties.

■ ASSOCIATED CONTENT

Supporting Information

The Supporting Information is available free of charge at https://pubs.acs.org/doi/10.1021/acs.cgd.1c00508.

AFM images, XRR and additional XRD measurements (PDF)

■ AUTHOR INFORMATION

Corresponding Authors

Roberto Mantovan − *Institute for Microelectronics and Microsystems, CNR-IMM Unit of Agrate Brianza, Agrate Brianza 20864, Italy;* orcid.org/0000-0002-9353-4137; Email: roberto.mantovan@mdm.imm.cnr.it

Massimo Longo − *Institute for Microelectronics and Microsystems, CNR-IMM Unit of Agrate Brianza, Agrate Brianza 20864, Italy;* Present Address: Institute for Microelectronics and Microsystems, CNR-IMM Unit of Rome, via Fosso del cavaliere, 100, 00133 Rome, Italy; orcid.org/0000-0002-6364-8184; Email: massimo.longo@artov.imm.cnr.it

Authors

Martino Rimoldi − *Institute for Microelectronics and Microsystems, CNR-IMM Unit of Agrate Brianza, Agrate Brianza 20864, Italy;* Present Address: CERN, European Organization for Nuclear Research, 1211, Geneva 23, Switzerland; orcid.org/0000-0002-2036-3648

Raimondo Cecchini − *Institute for Microelectronics and Microsystems, CNR-IMM Unit of Agrate Brianza, Agrate Brianza 20864, Italy;* Present Address: Institute for Microelectronics and Microsystems, CNR-IMM Unit of Bologna, via P. Gobetti 101, 40129, Bologna, Italy; orcid.org/0000-0003-3650-2478

Claudia Wiemer − *Institute for Microelectronics and Microsystems, CNR-IMM Unit of Agrate Brianza, Agrate Brianza 20864, Italy*

Emanuele Longo − *Institute for Microelectronics and Microsystems, CNR-IMM Unit of Agrate Brianza, Agrate Brianza 20864, Italy; Department of Material Science, University of Milano-Bicocca, Milan 20126, Italy*

Stefano Cecchi − *Institute for Microelectronics and Microsystems, CNR-IMM Unit of Agrate Brianza, Agrate Brianza 20864, Italy;* Present Address: Paul-Drude-Institut für Festkörperelektronik, Leibniz-Institut im Forschungsverbund Berlin e.V., Hausvogteiplatz 5-7, 10117 Berlin, Germany; orcid.org/0000-0002-2243-7268

Complete contact information is available at: https://pubs.acs.org/10.1021/acs.cgd.1c00508

Author Contributions

All authors have given approval to the final version of the manuscript.

Funding

This work was supported by the Horizon 2020 project SKYTOP "Skyrmion-Topological Insulator and Weyl Semi-metal Technology" (FETPROACT-2018-01, n. 824123).

Notes

The authors declare no competing financial interest.

■ REFERENCES

(1) Zhang, H.; Liu, C.-X.; Qi, X.-L.; Dai, X.; Fang, Z.; Zhang, S.-C. Topological insulators in Bi_2Se_3, Bi_2Te_3 and Sb_2Te_3 with a single Dirac cone on the surface. *Nat. Phys.* **2009**, *5*, 438−442.

(2) Bendt, G.; Zastrow, S.; Nielsch, K.; Mandal, P. S.; Sánchez-Barriga, J.; Rader, O.; Schulz, S. Deposition of topological insulator Sb_2Te_3 films by an MOCVD process. *J. Mater. Chem. A* **2014**, *2*, 8215−8222.

(3) Ginley, T. P.; Wang, Y.; Law, S. Topological Insulator Film Growth by Molecular Beam Epitaxy: A Review. *Crystals* **2016**, *6*, 154.

(4) Cecchini, R.; Mantovan, R.; Wiemer, C.; Nasi, L.; Lazzarini, L.; Longo, M. Weak Antilocalization in Granular Sb_2Te_3 Thin Films Deposited by MOCVD. *Phys. Status Solidi RRL* **2018**, *12*, No. 1800155.

(5) Longo, E.; Wiemer, C.; Cecchini, R.; Longo, M.; Lamperti, A.; Khanas, A.; Zenkevich, A.; Cantoni, M.; Rinaldi, C.; Fanciulli, M.; Mantovan, R. Fe/Sb_2Te_3 Interface Reconstruction through Mild Thermal Annealing. *Adv. Mater. Interfaces* **2020**, *7*, No. 2000905.

(6) Longo, E.; Wiemer, C.; Belli, M.; Cecchini, R.; Longo, M.; Cantoni, M.; Rinaldi, C.; Overbeek, M. D.; Winter, C. H.; Gubbiotti, G.; Tallarida, G.; Fanciulli, M.; Mantovan, R. Ferromagnetic resonance of Co thin films grown by atomic layer deposition on the Sb_2Te_3 topological insulator. *J. Magn. Magn. Mater.* **2020**, *509*, No. 166885.

(7) Lencer, D.; Salinga, M.; Grabowski, B.; Hickel, T.; Neugebauer, J.; Wuttig, M. A map for phase-change materials. *Nat. Mater.* **2008**, *7*, 972−977.

(8) Noé, P.; Vallée, C.; Hippert, F.; Fillot, F.; Raty, J.-Y. Phase-change materials for non-volatile memory devices: from technological

challenges to materials science issues. *Semicond. Sci. Technol.* **2018**, *33*, No. 013002.
(9) Venkatasubramanian, R.; Siivola, E.; Colpitts, T.; O'Quinn, B. Thin-film thermoelectric devices with high room-temperature figures of merit. *Nature* **2001**, *413*, 597−602.
(10) Ivanov, Y. V.; Burkov, A. T.; Pshenay-Severin, D. A. Thermoelectric Properties of Topological Insulators. *Phys. Status Solidi B* **2018**, *255*, No. 1800020.
(11) Zibouche, N.; Kuc, A.; Musfeldt, J.; Heine, T. Transition-metal dichalcogenides for spintronic applications. *Ann. Phys.* **2014**, *526*, 395−401.
(12) Longo, M.; Stoycheva, T.; Fallica, R.; Wiemer, C.; Lazzarini, L.; Rotunno, E. Au-catalyzed synthesis and characterization of phase change Ge-doped Sb-Te nanowires by MOCVD. *J. Cryst. Growth* **2013**, *370*, 323−327.
(13) Alegria, L. D.; Yao, N.; Petta, J. R. MOCVD synthesis of compositionally tuned topological insulator nanowires. *Phys. Status Solidi RRL* **2014**, *8*, 991−996.
(14) Rotunno, E.; Longo, M.; Wiemer, C.; Fallica, R.; Campi, D.; Bernasconi, M.; Lupini, A. R.; Pennycook, S. J.; Lazzarini, L. A Novel Sb_2Te_3 Polymorph Stable at the Nanoscale. *Chem. Mater.* **2015**, *27*, 4368−4373.
(15) Nminibapiel, D.; Zhang, K.; Tangirala, M.; Baumgart, H.; Chakravadhanula, V. S. K.; Kübel, C.; Kochergin, V. Growth of Nanolaminates of Thermoelectric Bi_2Te_3/Sb_2Te_3 by Atomic Layer Deposition. *ECS J. Solid State Sci. Technol.* **2014**, *3*, P95−P100.
(16) Saito, Y.; Fons, P.; Kolobov, A. V.; Tominaga, J. Self-organized van der Waals epitaxy of layered chalcogenide structures. *Phys. Status Solidi B* **2015**, *252*, 2151−2158.
(17) Saito, Y.; Fons, P.; Bolotov, L.; Miyata, N.; Kolobov, A. V.; Tominaga, J. A two-step process for growth of highly oriented Sb_2Te_3 using sputtering. *AIP Adv.* **2016**, *6*, No. 045220.
(18) Dong, G.-H.; Zhu, Y.-J.; Chen, L.-D. Sb_2Te_3 nanostructures with various morphologies: rapid microwave solvothermal synthesis and Seebeck coefficients. *CrystEngComm* **2011**, *13*, 6811−6816.
(19) Wang, G.; Zhu, X.; Wen, J.; Chen, X.; He, K.; Wang, L.; Ma, X.; Liu, Y.; Dai, X.; Fang, Z.; Jia, J.; Xue, Q. Atomically smooth ultrathin films of topological insulator Sb_2Te_3. *Nano Res.* **2010**, *3*, 874−880.
(20) Peranio, N.; Winkler, M.; Bessas, D.; Aabdin, Z.; König, J.; Böttner, H.; Hermann, R. P.; Eibl, O. Room-temperature MBE deposition, thermoelectric properties, and advanced structural characterization of binary Bi_2Te_3 and Sb_2Te_3 thin films. *J. Alloys Compd.* **2012**, *521*, 163−173.
(21) Kampmeier, J.; Weyrich, C.; Lanius, M.; Schall, M.; Neumann, E.; Mussler, G.; Schäpers, T.; Grützmacher, D. Selective area growth of Bi_2Te_3 and Sb_2Te_3 topological insulator thin films. *J. Cryst. Growth* **2016**, *443*, 38−42.
(22) Bonell, F.; Cuxart, M. G.; Song, K.; Robles, R.; Ordejón, P.; Roche, S.; Mugarza, A.; Valenzuela, S. O. Growth of Twin-Free and Low-Doped Topological Insulators on $BaF_2(111)$. *Cryst. Growth Des.* **2017**, *17*, 4655−4660.
(23) Pore, V.; Hatanpää, T.; Ritala, M.; Leskelä, M. Atomic Layer Deposition of Metal Tellurides and Selenides Using Alkylsilyl Compounds of Tellurium and Selenium. *J. Am. Chem. Soc.* **2009**, *131*, 3478−3480.
(24) Knapas, K.; Hatanpää, T.; Ritala, M.; Leskelä, M. In Situ Reaction Mechanism Studies on Atomic Layer Deposition of Sb_2Te_3 and GeTe from $(Et_3Si)_2Te$ and Chlorides. *Chem. Mater.* **2010**, *22*, 1386−1391.
(25) Pore, V.; Knapas, K.; Hatanpää, T.; Sarnet, T.; Kemell, M.; Ritala, M.; Leskelä, M.; Mizohata, K. Atomic Layer Deposition of Antimony and its Compounds Using Dechlorosilylation Reactions of Tris(triethylsilyl)antimony. *Chem. Mater.* **2011**, *23*, 247−254.
(26) Zastrow, S.; Gooth, J.; Boehnert, T.; Heiderich, S.; Toellner, W.; Heimann, S.; Schulz, S.; Nielsch, K. Thermoelectric transport and Hall measurements of low defect Sb_2Te_3 thin films grown by atomic layer deposition. *Semicond. Sci. Technol.* **2013**, *28*, No. 035010.
(27) Eom, T.; Gwon, T.; Yoo, S.; Choi, B. J.; Kim, M.-S.; Ivanov, S.; Adamczyk, A.; Buchanan, I.; Xiao, M.; Hwang, C. S. Chemical interaction and ligand exchange between a $[(CH_3)_3Si]_3Sb$ precursor and atomic layer deposited Sb_2Te_3 films. *J. Mater. Chem. C* **2015**, *3*, 1365−1370.
(28) Zheng, L.; Cheng, X.; Cao, D.; Wang, Q.; Wang, Z.; Xia, C.; Shen, L.; Yu, Y.; Shen, D. Direct growth of Sb_2Te_3 on graphene by atomic layer deposition. *RSC Adv.* **2015**, *5*, 40007−40011.
(29) Marchand, P.; Hassan, I. A.; Parkin, I. P.; Carmalt, C. J. Aerosol-assisted delivery of precursors for chemical vapour deposition: expanding the scope of CVD for materials fabrication. *Dalton Trans.* **2013**, *42*, 9406−9422.
(30) Benjamin, S. L.; de Groot, C. H.; Hector, A. L.; Huang, R.; Koukharenko, E.; Levason, W.; Reid, G. Chemical vapour deposition of antimony chalcogenides with positional and orientational control: precursor design and substrate selectivity. *J. Mater. Chem. C* **2015**, *3*, 423−430.
(31) Venkatasubramanian, R.; Colpitts, T.; O'Quinn, B.; Liu, S.; El-Masry, N.; Lamvik, M. Low-temperature organometallic epitaxy and its application to superlattice structures in thermoelectrics. *Appl. Phys. Lett.* **1999**, *75*, 1104−1106.
(32) Giani, A.; Boulouz, A.; Pascal-Delannoy, F.; Foucaran, A.; Charles, E.; Boyer, A. Growth of Bi_2Te_3 and Sb_2Te_3 thin films by MOCVD. *Mater. Sci. Eng.: B* **1999**, *64*, 19−24.
(33) Bendt, G.; Schulz, S.; Zastrow, S.; Nielsch, K. Single-Source Precursor-Based Deposition of Sb_2Te_3 Films by MOCVD**. *Chem. Vap. Deposition* **2013**, *19*, 235−241.
(34) Kuznetsov, P. I.; Shchamkhalova, B. S.; Yapaskurt, V. O.; Shcherbakov, V. D.; Luzanov, V. A.; Yakushcheva, G. G.; Jitov, V. A.; Sizov, V. E. MOVPE deposition of Sb_2Te_3 and other phases of Sb-Te system on sapphire substrate. *J. Cryst. Growth* **2017**, *471*, 1−7.
(35) Volykhov, A. A.; Sánchez-Barriga, J.; Sirotina, A. P.; Neudachina, V. S.; Frolov, A. S.; Gerber, E. A.; Kataev, E. Y.; Senkovsky, B.; Khmelevsky, N. O.; Aksenenko, A. Y.; Korobova, N. V.; Knop-Gericke, A.; Rader, O.; Yashina, L. V. Rapid Surface Oxidation of Sb_2Te_3 as Indication for a Universal Trend in the Chemical Reactivity of Tetradymite Topological Insulators. *Chem. Mater.* **2016**, *28*, 8916−8923.
(36) Venkatasubramanian, R.; Colpitts, T.; Watko, E.; Lamvik, M.; El-Masry, N. MOCVD of Bi_2Te_3, Sb_2Te_3 and their superlattice structures for thin-film thermoelectric applications. *J. Cryst. Growth* **1997**, *170*, 817−821.
(37) Longo, M.; Cecchi, S.; Selmo, S.; Fanciulli, M.; Wiemer, C.; Battaglia, J.; Saci, A.; Kusiak, A. *MOCVD growth and thermal analysis of Sb2Te3 thin films and nanowires*, NANOFIM 2015, 1st Workshop on Nanotechnology in Instrumentation and Measurement, Lecce, Italy, 24−25 July 2015, 150−154.
(38) Rimoldi, M.; Cecchini, R.; Wiemer, C.; Lamperti, A.; Longo, E.; Nasi, L.; Lazzarini, L.; Mantovan, R.; Longo, M. Epitaxial and large area Sb_2Te_3 thin films on silicon by MOCVD. *RSC Adv.* **2020**, *10*, 19936−19942.
(39) Boschker, J. E.; Momand, J.; Bragaglia, V.; Wang, R.; Perumal, K.; Giussani, A.; Kooi, B. J.; Riechert, H.; Calarco, R. Surface Reconstruction-Induced Coincidence Lattice Formation Between Two-Dimensionally Bonded Materials and a Three-Dimensionally Bonded Substrate. *Nano Lett.* **2014**, *14*, 3534−3538.
(40) Hilmi, I.; Lotnyk, A.; Gerlach, J. W.; Schumacher, P.; Rauschenbach, B. Research Update: Van-der-Waals epitaxy of layered chalcogenide Sb_2Te_3 thin films grown by pulsed laser deposition. *APL Mater.* **2017**, *5*, No. 050701.
(41) Bendt, G.; Kaiser, K.; Heckel, A.; Rieger, F.; Oing, D.; Lorke, A.; Rodriguez, N. P.; Schierning, G.; Jooss, C.; Schulz, S. Structural and thermoelectrical characterization of epitaxial Sb_2Te_3 high quality thin films grown by thermal evaporation. *Semicond. Sci. Technol.* **2018**, *33*, 105002.
(42) Kuznetsov, P. I.; Yakushcheva, G. G.; Luzanov, V. A.; Temiryazev, A. G.; Shchamkhalova, B. S.; Jitov, V. A.; Sizov, V. E. Metalorganic vapor phase epitaxy growth of ternary tetradymite $Bi_2Te_{3-x}Se_x$ compounds. *J. Cryst. Growth* **2015**, *409*, 56−61.
(43) Collins, J. L.; Tadich, A.; Wu, W.; Gomes, L. C.; Rodrigues, J. N. B.; Liu, C.; Hellerstedt, J.; Ryu, H.; Tang, S.; Mo, S.-K.; Adam, S.;

Yang, S. A.; Fuhrer, M. S.; Edmonds, M. T. Electric-field-tuned topological phase transition in ultrathin Na_3Bi. *Nature* **2018**, *564*, 390−394.
(44) Longo, E.; Belli, M.; Alia, M.; Rimoldi, M.; Cecchini, R.; Longo, M.; Wiemer, C.; Locatelli, L.; Gubbiotti, G.; Fanciulli, M.; Mantovan, R. Large spin-to-charge conversion at room temperature in extended epitaxial Sb_2Te_3 topological insulator chemically grown on Silicon. *ArXiv:2104.08124v1 [cond-mat.mtrl-sci]* 2021.
(45) Bansal, N.; Koirala, N.; Brahlek, M.; Han, M.-G.; Zhu, Y.; Cao, Y.; Waugh, J.; Dessau, D. S.; Oh, S. Robust topological surface states of Bi_2Se_3 thin films on amorphous SiO_2/Si substrate and a large ambipolar gating effect. *Appl. Phys. Lett.* **2014**, *104*, 241606.
(46) Jerng, S.-K.; Joo, K.; Kim, Y.; Yoon, S.-M.; Lee, J. H.; Kim, M.; Kim, J. S.; Yoon, E.; Chun, S.-H.; Kim, Y. S. Ordered growth of topological insulator Bi_2Se_3 thin films on dielectric amorphous SiO_2 by MBE. *Nanoscale* **2013**, *5*, 10618−10622.
(47) Wiesner, M.; Roberts, R. H.; Lin, J.-F.; Akinwande, D.; Hesjedal, T.; Duffy, L. B.; Wang, S.; Song, Y.; Jenczyk, J.; Jurga, S.; Mroz, B. The effect of substrate and surface plasmons on symmetry breaking at the substrate interface of the topological insulator Bi_2Te_3. *Sci. Rep.* **2019**, *9*, 6147.
(48) Wang, C. Y.; Lin, H. Y.; Yang, S. R.; Chen, K. H. M.; Lin, Y. H.; Chen, K. H.; Young, L. B.; Cheng, C. K.; Fanchiang, Y. T.; Tseng, S. C.; Hong, M.; Kwo, J. Demonstration of large field effect in topological insulator films via a high-κ back gate. *Appl. Phys. Lett.* **2016**, *108*, 202403.
(49) Hippert, F.; Kowalczyk, P.; Bernier, N.; Sabbione, C.; Zucchi, X.; Térébénec, D.; Mocuta, C.; Noé, P. Growth mechanism of highly oriented layered Sb_2Te_3 thin films on various materials. *J. Phys. D: Appl. Phys.* **2020**, *53*, 154003.
(50) Schuck, M.; Rieß, S.; Schreiber, M.; Mussler, G.; Grützmacher, D.; Hardtdegen, H. Metal organic vapor phase epitaxy of hexagonal Ge−Sb−Te (GST). *J. Cryst. Growth* **2015**, *420*, 37−41.
(51) Ratajczak, A.; von der Ahe, M.; Du, H.; Mussler, G.; Grützmacher, D. Metal organic vapor phase epitaxy of $Ge_1Sb_2Te_4$ thin films on Si(111) substrate. *Appl. Phys. A: Mater. Sci. Process.* **2019**, *125*, 163.
(52) *Inorganic crystal structure database (ICSD)*, Fitz Kahrlsruhe, file n° 2084 (2021)
(53) Richardella, A.; Kandala, A.; Lee, J. S.; Samarth, N. Characterizing the structure of topological insulator thin films. *APL Mater.* **2015**, *3*, No. 083303.

https://doi.org/10.1021/acs.cgd.1c00508
Cryst. Growth Des. 2021, 21, 5135−5144